ACS Catalysis

Research Article

pubs.acs.org/acscatalysis

Effect of Transition Metals on the Structure and Performance of the Doped Carbon Catalysts Derived From Polyaniline and Melamine for ORR Application

Hongliang Peng, Fangfang Liu, Xiaojun Liu, Shijun Liao,* Chenghang You, Xinlong Tian, Haoxiong Nan, Fan Luo, Huiyu Song, Zhiyong Fu, and Peiyan Huang

Key Lab for Fuel Cell Technology of Guangdong Province and Key Lab of New Energy Technology of Guangdong Universities, School of Chemistry and Chemical Engineering, South China University of Technology, Guangzhou 510641, China

Supporting Information

ABSTRACT: In this work, the effects of the addition of transition metals (Mn, Fe, Co, Ni, Cu) on the structure and performance of the doped carbon catalysts M-PANI/C-Mela are investigated. The results show that the doping of various transition metals affected structures and performances of the catalysts significantly. Doping with Fe and Mn leads to a catalyst with a graphene-like structure, and doping with Co, Ni, and Cu leads to a disordered or nanosheet structure. The doping of transition metals can enhance the performance of the catalysts, and their ORR activity follows the order of Fe > Co > Cu > Mn > Ni, which is consistent with the order of their active N contents. We suggest that the various performance enhancements of the transition metals may be the result of the joint effect of the following three aspects: the N content/active N content, metal residue, and the surface area and pore structure, but not the effect of any single factor.

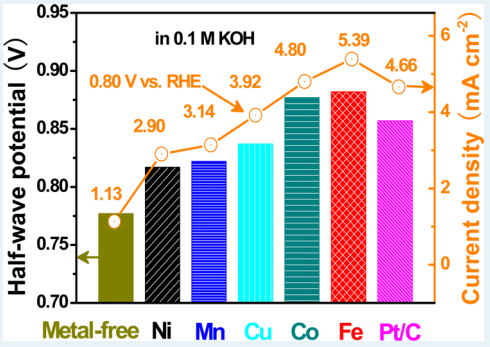

KEYWORDS: *doped carbon, effect, oxygen reduction reaction, performance, structure, transition metals*

1. INTRODUCTION

Doped carbon catalysts for oxygen reduction application have become one of the most attractive materials in the field of fuel cells recently, because their application will result in the sharp decrease in both the usage of precious platinum and the cost of fuel cells and will make the large-scale commercialization of fuel cells possible.[1] Great efforts have been made for developing a high-performance low-platinum[2−7] or a platinum-free doped carbon catalyst[8−14] and exploring the forming mechanism of active centers in the catalyst and the catalytic mechanism of oxygen reduction on the doped carbon catalysts.

It is recognized widely that the codoping of the transition metals would further enhance the performance of the catalyst based on enhancement of doped nitrogen. Many doped carbon catalysts with codoping of transition metals have been prepared and reported, and many efforts have been undertaken to reveal the role of transition metals for the performance enhancement of the catalysts.[15] In the initial experiments, the cobalt was codoped, and its improvement and role were investigated.[16−18] Recently, the codoping of late transition metals has been investigated widely. It has been found that the codoping of transition metals, especially codoping of Fe, could improve the ORR activity and stability. Although the importance of the codoping of transition metals has been verified and recognized by more and more researchers,[19−23] the issues related to the role and the action mechanism of the doped transition metals in a doped carbon catalyst, as well as the effects of various transition metals, still remains unclear.[24−26]

Choi et al.[27] prepared a series of nitrogen-doped carbon nanotube catalysts with codoping of Fe, Co, Ni, respectively, and investigated the effect of various transition metals on the performance of the catalysts. They found that the ORR activity of the catalysts follows the order of Co > Fe > Ni. They suggested that the doping of various transition metals might result in a different degree of sp^2-carbon network in the catalysts, thus causing various promotions. However, other researchers reported different promotion order for a different type of doped carbon catalyst. Zhang et al.[28] prepared a series of nitrogen-doped carbon-based catalysts with codoping of various transition metals. They found the ORR activity of the catalysts follows the order of Fe > Co > Zn > Mn > metal-free ≫Cu ≫ Ni, different from the order obtained by Choi et al.,[27] implying that the promotion of the transition metals may relate to the composition and structure of the catalysts. Behret et al.[29] studied the effect of nonprecious transition metal chalcogenide additives on the ORR activity, and they found the ORR activity of these compounds with an order of Co_3S_4 > Ni_3S_4 > Fe_3S_4. They suggested that empty (or half-empty) orbitals were playing a key role to back bonding with the π^*-electrons of the oxygen. Meanwhile, some theoretical studies on

Received: May 30, 2014
Revised: September 15, 2014
Published: September 16, 2014

   dx.doi.org/10.1021/cs500744x | ACS Catal. 2014, 4, 3797−3805

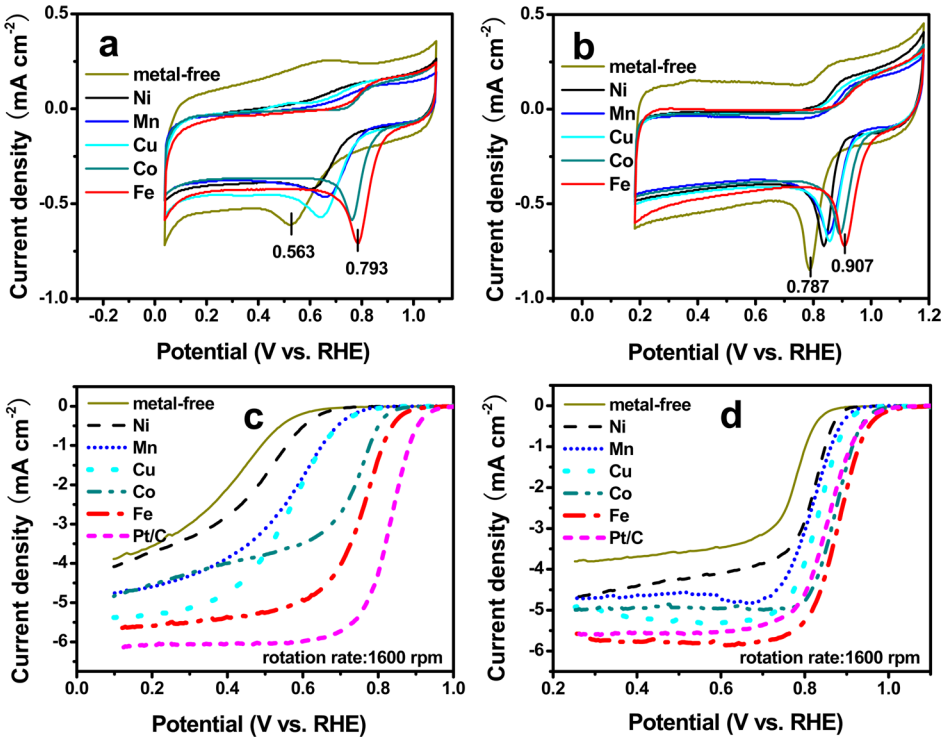

Figure 1. Cyclic voltammograms of M-PANI/C-Mela (M = Mn, Fe, Co, Ni and Cu) in O_2-saturated 0.1 M $HClO_4$ (a) and 0.1 M KOH (b). Linear-sweeping curves of JM Pt/C catalyst and M-PANI/C-Mela in O_2-saturated 0.1 M $HClO_4$ (c) and 0.1 M KOH (d) with a scanning rate of 5 mV s^{-1}.

the mechanism issue have been reported,[30−32] and recently, it was revealed by a density functional theory (DFT) calculation[31] that the adsorption behaviors of the catalysts doped with various transition metals were quite different, depending on the geometrical location of the active site, as well as the nearest neighbors and the oxidation state. Importantly, they suggested that the transition metals did not have intrinsic catalytic activities toward ORR.

Clearly, although some attempts have conducted, it is still a big challenge to understand or reveal the role and mechanism of codoped various transition metals in the doped carbon catalysts. Previously, we reported a high-performance doped carbon catalyst with codoping of Fe, which was prepared by pyrolyzing hybrid precursors of polyaniline, iron salt, and melamine,[33] and this catalyst exhibited excellent ORR activity and excellent H_2-air single PEM fuel cell performance. To investigate the effects of the codoping of various transition metals, in this work, we prepared a series of nitrogen doped carbon catalysts M-PANI/C-Mela with codoping of Mn, Fe, Co, Ni, Cu, respectively, and we investigated the effects of various transition metals codoped in catalysts on the structures and performances of the catalysts. We found that the codoping of various transition metals resulted in different structures, different surface areas, and different contents and distributions of active nitrogen, thus causing different improvements to the ORR performance of the catalysts.

2. EXPERIMENTAL SECTION

Preparation of Catalysts. A series of doped carbon catalyst M-PANI/C-Mela, in which various transition metals (MCl_x, M = Mn, Fe, Co, Ni, Cu) were codoped, respectively, was prepared with procedures reported previously by our group.[32,33] First, the hybrid precursors were prepared by the copolymerization of melamine, and aniline in the existence of transition metals salts, with ammonium peroxydisulfate (APS) as oxidant. Second, the doped carbon catalysts were prepared by pyrolyzing the precursors at 900 °C in an argon atmosphere for 1.0 h, followed by acid leaching with 0.5 M H_2SO_4 at 80 °C (typically: 1.0 g of catalyst powder per 50 mL of solution) for 10 h, annealing at 900 °C for 1 h.

Characterization of Catalysts. XRD was conducted on a TD-3500 powder diffractometer (Tongda, China) operated at 40 kV and 30 mA, using Cu Kα radiation sources. X-ray photoelectron spectroscopy (XPS) was performed on an ESCALAB MK2 X-ray photoelectron spectrometer (VG corporation, U.K.) employing a monochromated Al Kα X-ray source ($h\nu$ = 1486.6 eV). TEM images were recorded on a JEM-2100HR microscope (JEOL, Japan) operated at 200 kV. Brunauer−Emmett−Teller (BET) specific surface areas and pore distribution were measured on a Tristar II 3020 (Micromeritics, U.S.A.) gas adsorption analyzer. Raman analysis was performed on a LabRAM Aramis Raman spectrometer (HJY, France) with a laser wavelength of 532 nm.

Evaluation of Catalysts. ORR performances of the catalysts were evaluated on an electrochemical workstation (Ivium, Netherlands) at room temperature (25 ± 1 °C), using a three-electrode electrochemical setup. A graphite rod and Ag/AgCl (3 M KCl) were used as the counter and reference electrodes, respectively. The rotating ring disk electrode (RRDE) measurements were performed on a CHI 750E electrochemistry station (CH Instruments, U.S.A.) and an MSR speed controller (Pine Research Instrumentation, U.S.A.); the ring potential was set to 0.5 V. The potential of the reference electrode is corrected with the reversible hydrogen electrode (RHE), in 0.1 M KOH, E (RHE) = E (Ag/AgCl) + 0.982 V; in 0.1 M $HClO_4$, E (RHE) = E (Ag/AgCl) + 0.288 V.

All the catalyst electrodes were prepared by the methods reported in the literature.[34] For doped carbon catalysts, the loading of the catalyst is 0.51 mg cm^{-2}. JM Hispec 4100 Pt/C

dx.doi.org/10.1021/cs500744x | ACS Catal. 2014, 4, 3797−3805

Table 1. ORR Kinetic Data for M-PANI/C-Mela Catalysts

catalyst	ORR onset potential (V)[c]		half-wave potential (V)		Tafel slope (mV dec^{-1})		J (mA cm^{-2})		J_{kin} (mA cm^{-2})		electron transfer number (n)	
metal-free	0.68[a]	0.86[b]	0.41[a]	0.78[b]	133[a]	59[b]	0.04[d]	1.13[e]	0.04[d]	1.42[e]	3.37[a]	3.13[b]
Mn-PANI/C-Mela	0.78	0.92	0.56	0.82	110	66	0.45	3.14	0.48	7.03	3.73	3.85
Fe-PANI/C-Mela	0.91	1.01	0.76	0.88	72	70	4.08	5.39	12.72	75.19	3.95	4.10
Co-PANI/C-Mela	0.86	0.97	0.72	0.87	67	64	2.76	4.80	5.10	30.62	3.45	3.73
Ni-PANI/C-Mela	0.70	0.89	0.48	0.81	116	50	0.06	2.90	0.06	5.93	3.33	3.50
Cu-PANI/C-Mela	0.80	0.93	0.56	0.84	116	64	0.48	3.92	0.52	12.59	3.90	3.80

[a]The data in the column from 0.1 M $HClO_4$ solution. [b]The data in the column from 0.1 M KOH solution. [c]The potential of the current density of ca. 0.05 mA cm^{-2}. [d]The current densities at 0.70 V (vs RHE) in 0.1 M $HClO_4$. [e]The current densities at 0.8 V (vs RHE) 0.1 M KOH.

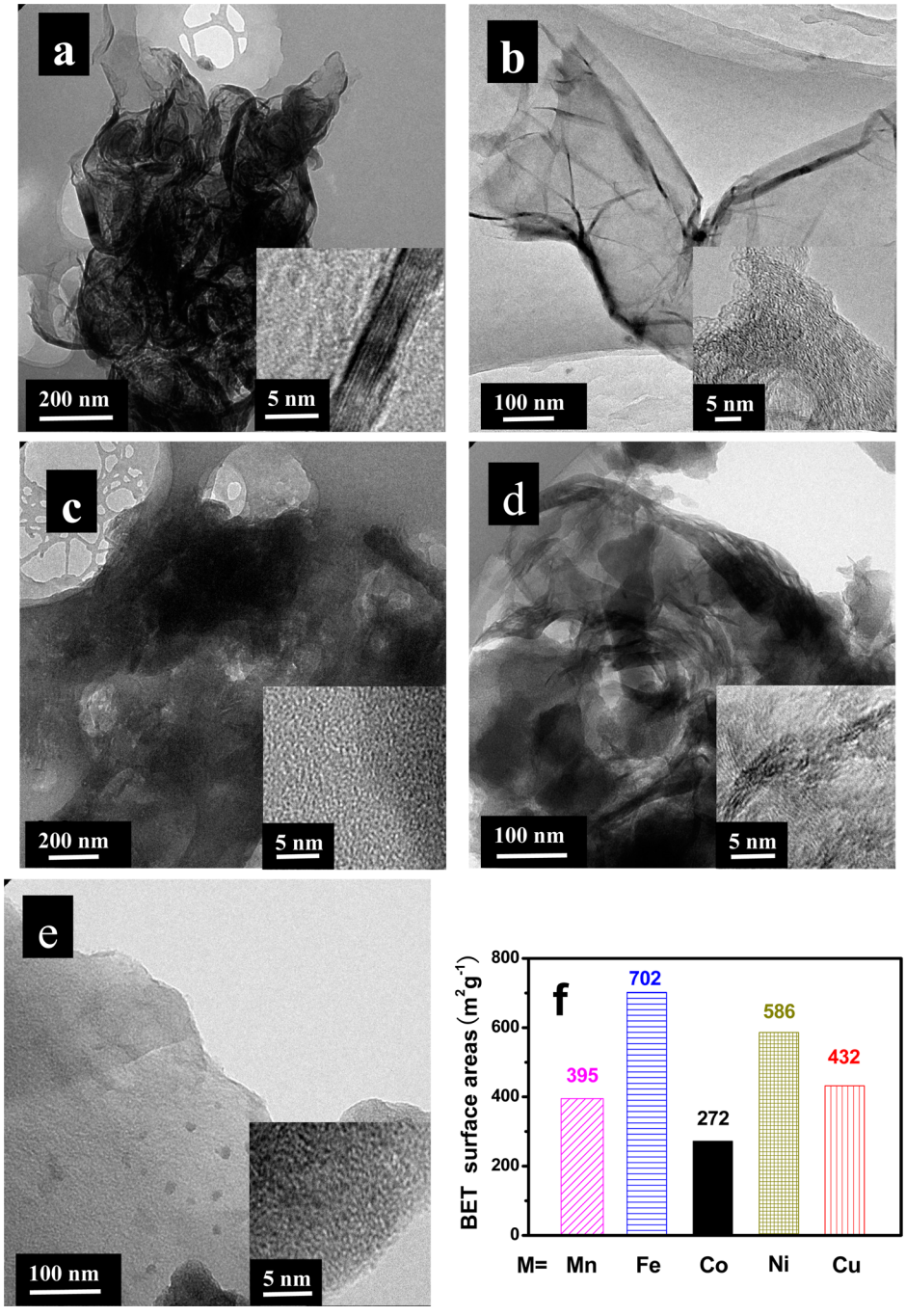

Figure 2. TEM images of (a) Mn-PANI/C-Mela, (b) Fe-PANI/C-Mela, (c) Co-PANI/C-Mela, (d) Ni-PANI/C-Mela, and (e) Cu-PANI/C-Mela; BET surface areas of these catalysts (f).

dx.doi.org/10.1021/cs500744x | ACS Catal. 2014, 4, 3797−3805

catalysts were used for the comparison; the loading of the catalyst is 25 μg Pt cm^{-2}.

3. RESULTS AND DISCUSSION

3.1. ORR Activity. Transition metal doping is an effective method to improve ORR activity.[35−37] As shows in Figure 1, doping of transition metals can enhance the ORR activity of the catalysts significantly, and the catalysts doped with various transition metals exhibit different performance enhancements. As shown in Figure 1a−d, the ORR onset potential for M-PANI/C-Mela follows the order of Fe > Co > Cu > Mn > Ni > metal-free in both acidic and alkaline mediums. Figure 1c,d show that the catalysts doped with various metals exhibits quite different ORR performance, including different onset potential and different half-wave potential. Interestingly, the limiting current densities measured with various catalysts are also significantly different. It may be caused by following two aspects: one is the four electron selectivity—the catalyst with higher four electron selectivity exhibits higher limiting current density; another is the activity of the catalysts—the catalyst with higher ORR activity generally exhibits higher limiting current density. In both acidic and alkaline mediums, Fe codoped catalyst exhibited best ORR activity, and Ni codoped catalyst exhibited worst ORR activity. Actually, this order also is consistent with the orders of their ORR onset potential, half-wave potential, and kinetic current density (J_{kin}) (see Table 1).

It should be pointed out that the graphene-like structured catalyst exhibits significantly superior activity than the doped carbon catalyst with normal disorder structures. For example, our graphene-like Fe-PANI/C-Mela catalyst shows much higher ORR performance than the Fe-Mel-CPS catalyst reported previously by literature, with similar nitrogen and Fe contents but without graphene-like structures.[38]

As shown in Table 1, the Fe-doped catalyst has the largest electron transfer numbers in both acidic and alkaline media. However, the metal-free catalyst has the lowest electron transfer number in alkaline medium and nearly the lowest number in the acidic medium. These results imply that the catalysts doped with various transition metals have varied four-electron selectivity, and the Fe doped catalyst has the highest four-electron selectivity. It is important that the kinetic current density of the Fe-doped catalyst is 200 times higher than that of the Ni-doped catalyst in the acidic medium and over 10 times higher in the alkaline medium, revealing the excellent intrinsic activity of the Fe-doped catalyst. We are not presently able to explain the reason for this performance, so it requires further investigation.

3.2. Morphologies and Surface Areas of the Catalysts. Figure 2a−e shows the TEM images of M-PANI/C-Mela catalysts. We found that the structure and morphology of the catalysts are affected strongly by the codoping of various transition metals. The Fe-PANI/C-Mela and Mn-PANI/C-Mela samples look like gauze, with graphene or graphene-like structures. However, the Co-PANI/C-Mela, Ni-PANI/C-Mela, and Cu-PANI/C-Mela samples show disordered carbon, nanosheets, graphite, or mixed structures. It is clearly that the codoping with various transition metals will result in various structures and morphologies, and this conclusion is supported by the Raman analysis results (see Supporting Information Figure S5), in which the catalysts exhibits obviously different peak shifts and different ratio of I_D/I_G.

Why does doping with various transition metals cause various structures and morphology? We suggest the following likely factors: One factor is that the various various transition metals (e.g., Fe^{3+}), when they form complexes with melamine and polyaniline, probably adapt coordination numbers of 4 to form planar macromolecules. However, Ni^{2+} and Co^{2+} may adapt the coordination number of 6 to form a cubic three-dimensional macromolecule, thereby resulting in the different structures and morphologies. The second is that variable catalysis of various transition metals toward the pyrolysis of mixture of melamine and polyaniline are due to their various d electron structures.

To further study the effects of various transition metals, we measured the surface area of five samples through the N_2 adsorption/desorption method (Figure 3a) and found that the

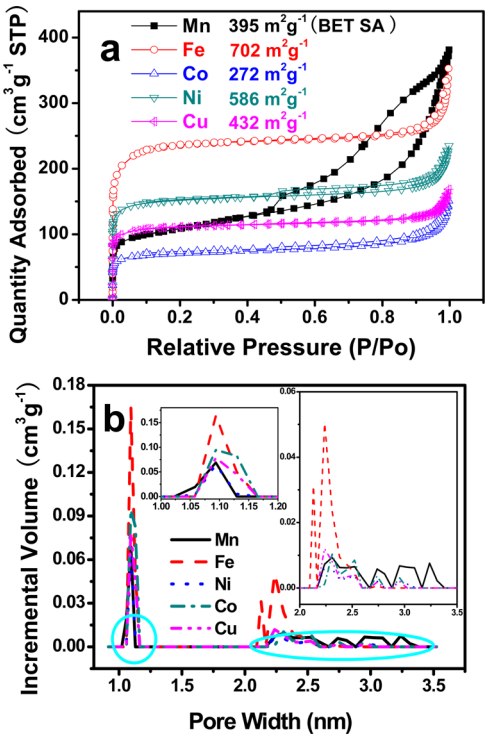

Figure 3. (a) N_2 sorption/desorption isotherms of doped carbon catalysts codoped with various transition metals; (b) Pore-size distribution curves of doped carbon catalysts codoped with various transition metals. Density functional theory adsorption pore distribution (pore width from 0.9 to 3.5 nm).

surface areas of five samples, codoped with Fe, Co, Ni, Mn, Cu, respectively, follows the order of Fe > Ni > Cu >Mn > Co. The catalyst with codoping of Fe exhibited the highest surface area (702 m^2/g); this can be attributed to its graphene-like structure, resulting from the macroplanar structure of the four-coordinated Fe complex and its porous structure (see Figure 3b).

When comparing the performance order of five catalysts, we can see that the ORR performance order of five catalysts is not exactly consistent with their surface areas order. For example, the Fe-doped catalyst has the highest surface area and the highest ORR performance, but the Ni-doped catalyst has the second highest surface area and the lowest ORR performance. Clearly, this increase in surface area may be an important factor for the performance enhancement, but it is not the decisive factor.

If we normalized the activity to the BET surface area (see Supporting Information Figure S6), we find that the Co-doped catalyst, but not the Fe doped catalyst, exhibits the highest specific surface area activity toward the ORR. In addition, the Ni-doped catalyst exhibits the lowest specific surface area activity,

dx.doi.org/10.1021/cs500744x | ACS Catal. 2014, 4, 3797−3805

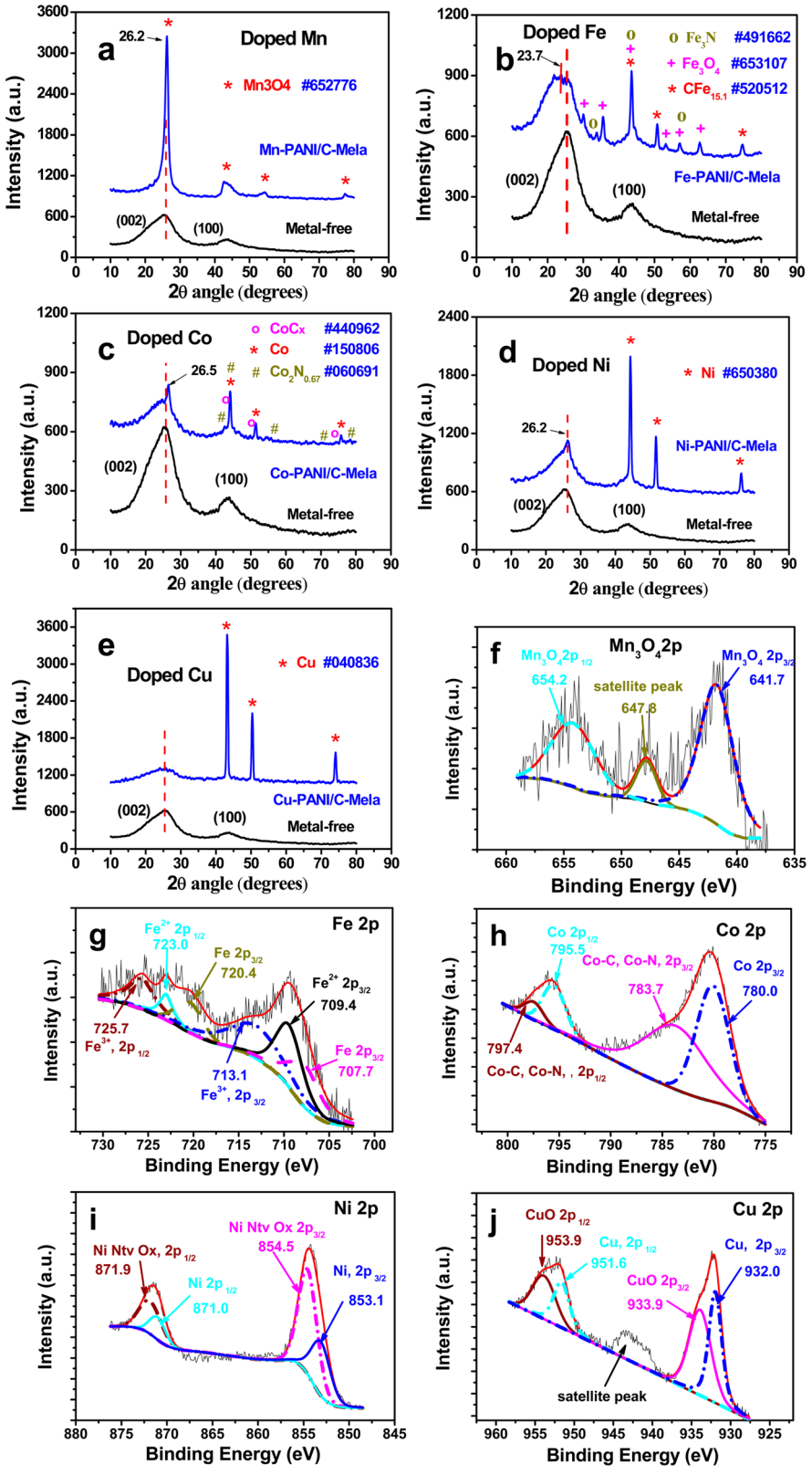

Figure 4. XRD and XPS patterns of Mn-PANI/C-Mela (a, f), Fe-PANI/C-Mela (b, g), Co-PANI/C-Mela (c, h), Ni-PANI/C-Mela (d, (i), and Cu-PANI/C-Mela (e, j).

revealing that Co-doped catalyst may have the highest activity center density, while the Ni-doped catalyst has the lowest.

As shown in Figure 3b, all five catalysts have almost same micropore size (ca. 1.1−1.2 nm) and almost the same mesopore size (ca. 2.2−2.6 nm). However, they have obviously different pore volumes. The Fe-codoped catalyst shows the largest pore volumes at micropore size. It is interesting that the order of micropore volumes for our catalysts is quite consistent with the

dx.doi.org/10.1021/cs500744x | ACS Catal. 2014, 4, 3797−3805

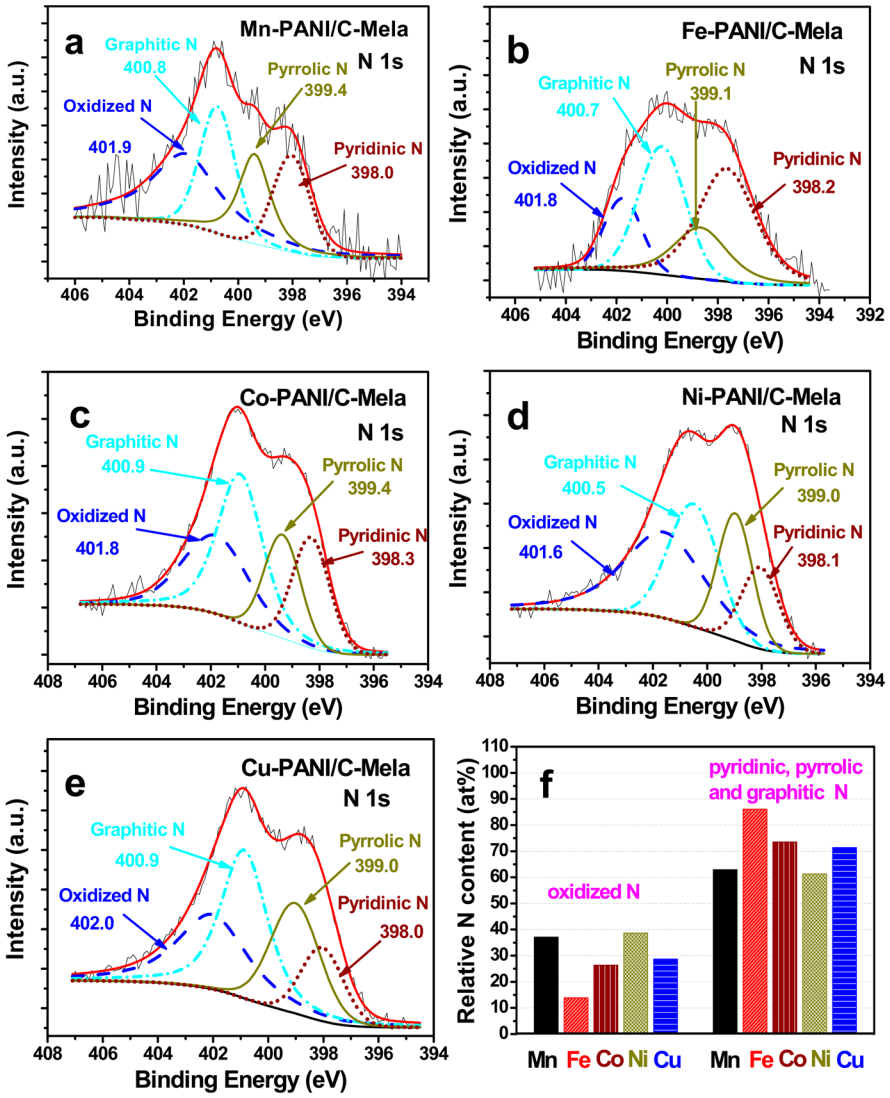

Figure 5. High-resolution XPS spectra of N 1s of (a) Mn-PANI/C-Mela, (b) Fe-PANI/C-Mela, (c) Co-PANI/C-Mela, (d) Ni-PANI/C-Mela, (e) Cu-PANI/C-Mela; (f) the relative N content (atom %) of oxidized N and the sum of pyridinic, pyrrolic, and graphitic N.

ORR performance order. Thus, it seems to be an important factor affecting the ORR performance of the catalysts. Actually, Dodelet et al.[39−41] suggested that micropores might host most of the catalytic sites in their heat-treated Fe/N/C catalysts previously.

3.3. Existences of Various Transition Metals in Doped Carbon Catalysts. Figure 4a−e show the XRD patterns of five catalyst samples codoped with Mn, Fe, Co, Ni, and Cu, respectively, and we were surprised to find that various doped metals existed in different chemical states. For the Mn-codoped catalyst, a strong diffraction peak at 2θ of 26.2° could be assigned to the (211) peak of Mn_3O_4, which is supported by the results of XPS (Figure 4f), in which two peaks at 641.7 and 654.2 eV correspond to the Mn $2p_{3/2}$ and Mn $2p_{1/2}$ spin orbit peaks of Mn_3O_4 (Figure 4f).[42] However, for the Fe-doped catalyst, Fe exists as Fe, Fe_3N, Fe_3O_4, and $CFe_{15.1}$(austenite), as shown by the XRD results (Figure 4b), and the XPS spectrum also revealed that the Fe exists with Fe(0), Fe(II), and Fe(III), with relative contents of 28, 32, and 40 atom %, respectively. By XRD results, cobalt exists in the Co-PANI/C-Mela with metal Co, cobalt carbide (CoCx), and cobalt nitride ($Co_{5.47}N$). The XPS spectrum of Co revealed that the peaks at 780.0 (795.5) and 783.7 (797.4) eV correspond to the Co and cobalt compounds (Co−C or Co−N),[43] respectively. Contents of metal Co and cobalt compounds are 46−54 atom %. It is interesting that only elemental metallic Ni, Cu are detected by XRD in the Ni- and Cu-doped catalysts. According to the deconvolution results of the XPS spectra of Ni- and Cu-doped catalysts (Figure 4i,j), there should be some oxides of Ni and Cu in the Ni-PANI/C-Mela and Cu-PANI/C-Mela catalysts, respectively.

As we mentioned previously,[33,34,44] doped transition metals may have two roles: one is as a catalyst for the formation of stable active sites in the pyrolysis process and the other is that the residual metal compounds serve as active sites directly. With regard to the catalytic activity of residual metal compounds toward the oxygen reduction reaction, according to the literature and our experiments results, metals oxide may not contribute to the ORR activity enhancement of the catalyst significantly. We guess this may be one of the reasons that the Mn-doped catalyst exhibited inferior ORR performance compared with other metal-doped catalysts, because Mn exists only as an oxide in the catalyst. Elemental metal may contribute to the enhancement of performance weakly; it may be reasoned that Ni- or Cu-codoped catalysts exhibited slight enhancements of ORR performance.

dx.doi.org/10.1021/cs500744x | ACS Catal. 2014, 4, 3797−3805

Table 2. Contents of Residue Metal, Total Nitrogen and Active Nitrogen of M-PANI/C-Mela Catalysts Doped with Various Transition Metals, Determined by the XPS Analysis

		final surface nitrogen content (atom %)		relative content (%) of N				
sample	final surface metal content (atom %)	total N	active N	N—"O"	graphitic N	pyrrolic N	pyridinic N	sum of active N
Mn-PANI/C-Mela	0.40	1.3	0.8	37.1	25.2	19.5	18.2	62.9
Fe-PANI/C-Mela	0.68	1.9	1.6	13.9	30.5	17.4	38.2	86.1
Co-PANI/C-Mela	1.38	1.5	1.1	26.4	37.1	17.4	19	73.5
Ni-PANI/C-Mela	0.70	4.0	2.5	38.7	27.8	19.8	13.7	61.3
Cu-PANI/C-Mela	1.74	3.8	2.7	28.7	35.7	23	12.7	71.4

According to this work, the existence of nitride and carbide of transition metals may form new ORR active sites for the catalysts, which will enhance the performance of the catalyst remarkably. Superior ORR performances of Fe- or Co-codoped catalysts may partly result in the contribution of the active sites formed on the nitride and carbide of Fe and Co.[36,45]

It is worthwhile to note that the diffraction peak of graphite (002) shifted with the addition of various transition metals. This implies that the structures of the doped carbon catalysts are affected strongly by the various codoped transition metals. We observe that this peak varied from 23.3 for the Fe-doped catalyst to 26.5 for the Co-doped catalyst. It further confirmed that the structures of the doped carbon catalyst could be affected by the addition of various types of transition metals.

3.4. XPS Analysis of Doped Nitrogen in the Catalysts. To study the effect of various transition metals on the doping of nitrogen, we analyzed the N distribution of the five catalysts with XPS and deconvolution methods. Figure 5a–e show the XPS spectra of N 1s for the five catalysts doped with Mn, Fe, Co, Ni, and Cu. Their deconvoluting spectra of N 1s spectrum for each sample show in the each spectrum. Generally, four peaks at 398.0 ± 0.4, 399.4 ± 0.4, 400.8 ± 0.4, and 402.0 ± 0.4 eV can be assigned to pyridinic N,[46] pyrrolic N,[47] graphitic N,[48] and oxidized N species,[49] respectively. Pyridinic, pyrrolic, and graphitic N are recognized as active N species toward ORR.[50−53]

We calculated the relative contents of active nitrogen species and oxidized nitrogen species from Figure 5a–d and list the results in Figure 5f. From Figure 5f, we can see that the relative contents of active N species are different with respect to the various codoped transition metals. The Fe-codoped catalyst has the highest relative content of active nitrogen, and the Ni-codoped catalyst has the lowest content of relatively active nitrogen. Furthermore, we find that the order of relative contents of active nitrogen in five catalysts is consistent with their ORR order; it seems that the active N species is an important factor affected the performance of the doped catalysts. However, it should be pointed out that the order of absolute N content and the order of absolute active N content are entirely inconsistent with the catalyst's ORR performance order at all (see Table 2). The Ni-doped catalyst has the highest N content and the second highest active N content, but it has the lowest ORR performance in the five catalysts.

Clearly, we cannot simply correlate the ORR performance with the surface N content, or the active N content, or any single factor. The ORR performance of the catalysts doped with transition metals may be affected by the N content/active N content, metal residue, surface area, pore structure, and other qualities.

3.5. Effect of Metal Residue on the ORR Performance. As we described above, we believe the transition metal residues may play an important role for enhanced performances of these catalysts. To verify it, we attempt to identify the role of metal residue in our M-PANI/C-Mela catalysts by removing the metal residues from catalysts with 37 wt % HCl at 80 °C for 24 h. Figure 6

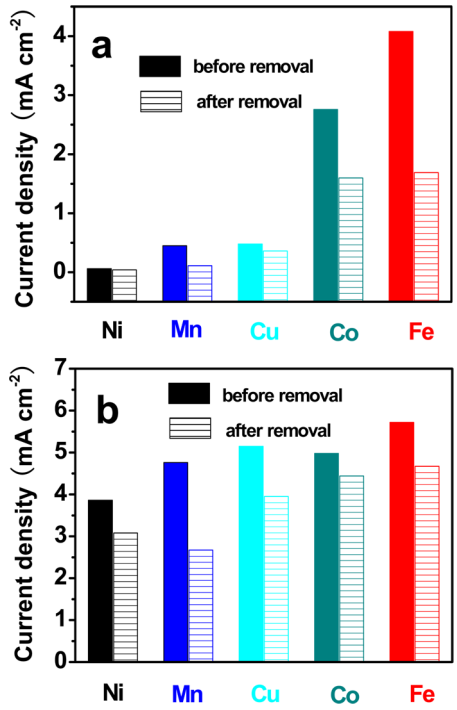

Figure 6. Current density at 0.7 V of M-PANI/C-Mela catalysts before and after removal of transition metal residues in O_2-saturated (a) 0.1 M $HClO_4$ and (b) 0.1 M KOH. Rotation rate: 1600 rpm; scanning rate: 5 mV s^{-1}.

presents the ORR performances of the catalysts before and after removal of metal residues, and it is clear that all five catalyst exhibit reduced performance after the removal of metals residues by boiling in acidic chloride, revealing that the metal residues play an important role for the enhanced performances of the catalysts. However, the fading extents of ORR performances for five catalysts are quite different. For Fe-PANI/C-Mela catalysts (Figure 6a), after removal of Fe residues, its ORR current density at 0.7 V (vs RHE) decreased from 4.1 to 1.7 mA cm^{-2}, a 63% of performance loss in acidic medium. However, for Co-PANI/C-Mela, the decrease was from 2.8 to 1.6 mA cm^{-2}, a performance loss of ca. 43%, revealing that the promotions of different transition metals residues are quite different. In alkaline medium (Figure 6b), the performance loss caused by the removal of Mn is larger than that caused by the removal of Cu and Ni, further confirming that the performance contribution of the residues of various transition metals is quite different.

A schematic diagram describing the formation process of the M and N codoped carbon catalyst with different structures is

dx.doi.org/10.1021/cs500744x | ACS Catal. 2014, 4, 3797−3805

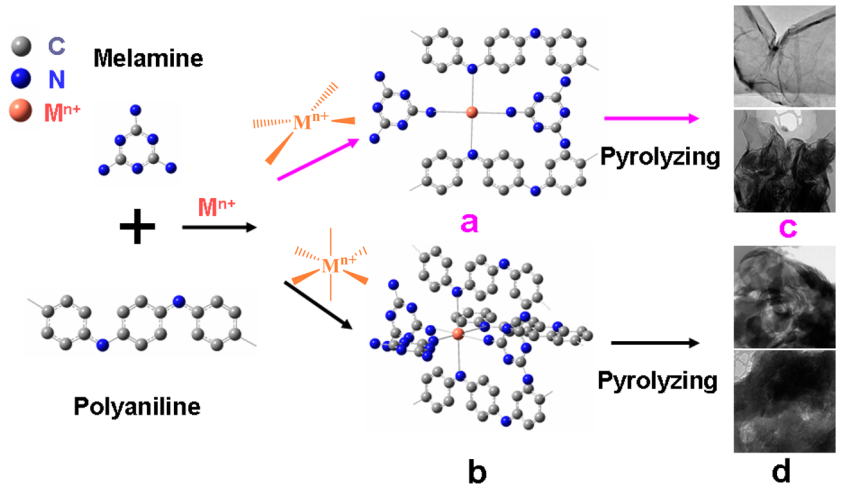

Figure 7. Schematic diagram of the formation processes of the transition metals and nitrogen codoped carbon catalysts with different structures.

suggested (see Figure 7). Simply, transition metal ions may combine with polyaniline and melamine to form two types of complexes: four-coordinated planar structured complex macromolecule (step a) and six-coordinated cubic three-dimension macromolecule (step b). For example, Fe may form a four-coordinated complex with polyaniline and melamine, but Ni may form a six-coordinated complex. During pyrolysis, the planar complex macromolecules may transform into graphene-like structured doped carbon catalyst following step c. Three-dimensional complex macromolecules may transform into three-dimensional carbon catalyst following the step d. Conclusively, the different morphologies of the doped carbon catalysts with different transition metals may be caused by the different coordination number of the transition metals, as well as the different stereo structures of the complex molecules with various transition metals.

4. CONCLUSIONS

In conclusion, the effects of doping transition metals on the structure and performance of doped carbon catalysts M-PANI/C-Mela (M = Mn, Fe, Co, Ni, Cu) were investigated. All the transition metal codoped catalysts exhibited various enhancing extents to ORR performance. Doping with various transition metals will result in a variety of morphologies, surface areas, pore structures, metal residues, active nitrogen contents, and active nitrogen distributions. We suggest that the performance enhancement resulted from a combination of these factors rather than any single factor.

■ ASSOCIATED CONTENT

Supporting Information

Theoretical, Koutecky–Levich analysis, H_2O_2 yield, Tafel plots analysis, Raman analysis, and specific surface area activity analysis. This material is available free of charge via the Internet at http://pubs.acs.org.

■ AUTHOR INFORMATION

Corresponding Author

*E-mail: chsjliao@scut.edu.cn. Fax +86 20 87113586.

Notes

The authors declare no competing financial interest.

■ ACKNOWLEDGMENTS

The authors would like to acknowledge the financially supported of the National Science Foundation of China (NSFC Project Nos. 21076089, 21276098, 11132004, U1301245), the Ministry of Science and Technology of China (Project No. 2012AA053402), the Guangdong Natural Science Foundation (Project No. S2012020011061), the Doctoral Fund of the Ministry of Education of China (No. 20110172110012), and the Basic Scientific Foundation of the Central Universities of China (No. 2013ZP0013).

■ REFERENCES

(1) Debe, M. K. *Nature* **2012**, *486*, 43−51.
(2) Feng, Y. Y.; Zhang, G. R.; Ma, J. H.; Liu, G.; Xu, B. Q. *Phys. Chem. Chem. Phys.* **2011**, *13*, 3863−3872.
(3) Sun, S.; Zhang, G.; Gauquelin, N.; Chen, N.; Zhou, J.; Yang, S.; Chen, W.; Meng, X.; Geng, D.; Banis, M. N.; Li, R.; Ye, S.; Knights, S.; Botton, G. A.; Sham, T. K.; Sun, X. *Sci. Rep.* **2013**, *3*, 1775.
(4) Liao, S.; Holmes, K. A.; Tsaprailis, H.; Birss, V. I. *J. Am. Chem. Soc.* **2006**, *128*, 3504−3505.
(5) Yang, L.; Vukmirovic, M. B.; Su, D.; Sasaki, K.; Herron, J. A.; Mavrikakis, M.; Liao, S.; Adzic, R. R. *J. Phys. Chem. C* **2013**, *117*, 1748−1753.
(6) Wang, R.; Wang, H.; Li, H.; Wang, W.; Key, J.; Khotseng, L.; Ji, S. *Electrochim. Acta* **2014**, *132*, 251−257.
(7) Kang, Y.; Ye, X.; Chen, J.; Cai, Y.; Diaz, R. E.; Adzic, R. R.; Stach, E. A.; Murray, C. B. *J. Am. Chem. Soc.* **2013**, *135*, 42−45.
(8) Ding, W.; Wei, Z.; Chen, S.; Qi, X.; Yang, T.; Hu, J.; Wang, D.; Wan, L. J.; Alvi, S. F.; Li, L. *Angew. Chem.* **2013**, *125*, 11971−11975.
(9) Ramaswamy, N.; Tylus, U.; Jia, Q.; Mukerjee, S. *J. Am. Chem. Soc.* **2013**, *135*, 15443−15449.
(10) Kim, B. J.; Lee, D. U.; Wu, J.; Higgins, D.; Yu, A.; Chen, Z. *J. Phys. Chem. C* **2013**, *117*, 26501−26508.
(11) Sun, X.; Song, P.; Chen, T.; Liu, J.; Xu, W. *Chem. Commun.* **2013**, *49*, 10296−10298.
(12) Sheng, Z. H.; Shao, L.; Chen, J. J.; Bao, W. J.; Wang, F. B.; Xia, X. H. *ACS Nano* **2011**, *5*, 4350−4358.
(13) Liu, F.; Peng, H.; You, C.; Fu, Z.; Huang, P.; Song, H.; Liao, S. *Electrochim. Acta* **2014**, *138*, 353−359.
(14) Sun, X.; Zhang, Y.; Song, P.; Pan, J.; Zhuang, L.; Xu, W.; Xing, W. *ACS Catal.* **2013**, *3*, 1726−1729.
(15) Rabis, A.; Rodriguez, P.; Schmidt, T. J. *ACS Catal.* **2012**, *2*, 864−890.
(16) Jasinski, R. *Nature* **1964**, *201*, 1212−1213.
(17) Bashyam, R.; Zelenay, P. *Nature* **2006**, *443*, 63−66.

(18) Liang, Y.; Li, Y.; Wang, H.; Zhou, J.; Wang, J.; Regier, T.; Dai, H. *Nat. Mater.* **2011**, *10*, 780−786.
(19) Wu, G.; Johnston, C. M.; Mack, N. H.; Artyushkova, K.; Ferrandon, M.; Nelson, M.; Lezama-Pacheco, J. S.; Conradson, S. D.; More, K. L.; Myers, D. J.; Zelenay, P. *J. Mater. Chem.* **2011**, *21*, 11392−11405.
(20) Chung, H. T.; Won, J. H.; Zelenay, P. *Nat. Commun.* **2013**, *4*, 1922.
(21) Yan, X. H.; Xu, B. Q. *J. Mater. Chem. A* **2014**, *2*, 8617−8622.
(22) Wu, G.; More, K. L.; Johnston, C. M.; Zelenay, P. *Science* **2011**, *332*, 443−447.
(23) Deng, D.; Yu, L.; Chen, X.; Wang, G.; Jin, L.; Pan, X.; Deng, J.; Sun, G.; Bao, X. *Angew. Chem., Int. Ed.* **2013**, *52*, 371−375.
(24) Chen, Z.; Higgins, D.; Yu, A.; Zhang, L.; Zhang, J. *Energy Environ. Sci.* **2011**, *4*, 3167−3192.
(25) Yu, D.; Nagelli, E.; Du, F.; Dai, L. *J. Phys. Chem. Lett.* **2010**, *1*, 2165−2173.
(26) Sun, X.; Song, P.; Zhang, Y.; Liu, C.; Xu, W.; Xing, W. *Sci. Rep.* **2013**, *3*, 2505.
(27) Choi, C. H.; Park, S. H.; Woo, S. I. *Appl. Catal., B* **2012**, *119*, 123−131.
(28) Zhang, H. J.; Jiang, Q. Z.; Sun, L.; Yuan, X.; Shao, Z.; Ma, Z. F. *Int. J. Hydrogen Energy* **2010**, *35*, 8295−8302.
(29) Behret, H.; Binder, H.; Sandstede, G. *Electrochim. Acta* **1975**, *20*, 111−117.
(30) Kattel, S.; Atanassov, P.; Kiefer, B. *Phys. Chem. Chem. Phys.* **2013**, *15*, 148−153.
(31) Calle-Vallejo, F.; Ignacio Martinez, J.; Rossmeisl, J. *Phys. Chem. Chem. Phys.* **2011**, *13*, 15639−15643.
(32) Yu, L.; Pan, X.; Cao, X.; Hu, P.; Bao, X. *J. Catal.* **2011**, *282*, 183−190.
(33) Peng, H.; Mo, Z.; Liao, S.; Liang, H.; Yang, L.; Luo, F.; Song, H.; Zhong, Y.; Zhang, B. *Sci. Rep.* **2013**, *3*, 1765.
(34) Peng, H.; Hou, S.; Dang, D.; Zhang, B.; Liu, F.; Zheng, R.; Luo, F.; Song, H.; Huang, P.; Liao, S. *Appl. Catal., B* **2014**, *158−159*, 60−69.
(35) Jaouen, F.; Proietti, E.; Lefèvre, M.; Chenitz, R.; Dodelet, J. P.; Wu, G.; Chung, H. T.; Johnston, C. M.; Zelenay, P. *Energy environ. Sci.* **2011**, *4*, 114−130.
(36) Ferrandon, M.; Kropf, A. J.; Myers, D. J.; Artyushkova, K.; Kramm, U.; Bogdanoff, P.; Wu, G.; Johnston, C. M.; Zelenay, P. *J. Phys. Chem. C* **2012**, *116*, 16001−16013.
(37) Cheon, J. Y.; Kim, T.; Choi, Y.; Jeong, H. Y.; Kim, M. G.; Sa, Y. J.; Kim, J.; Lee, Z.; Yang, T. H.; Kwon, K.; Terasaki, O.; Park, G. G.; Adzic, R. R.; Joo, S. H. *Sci. Rep.* **2013**, *3*, 2715.
(38) You, C.; Liao, S.; Qiao, X.; Zeng, X.; Liu, F.; Zheng, R.; Song, H.; Zeng, J.; Li, Y. *J. Mater. Chem. A* **2014**, *2*, 12240−12246.
(39) Jaouen, F.; Lefèvre, M.; Dodelet, J. P.; Cai, M. *J. Phys. Chem. B* **2006**, *110*, 5553−5558.
(40) Lefevre, M.; Proietti, E.; Jaouen, F.; Dodelet, J. P. *Science* **2009**, *324*, 71−74.
(41) Proietti, E.; Jaouen, F.; Lefèvre, M.; Larouche, N.; Tian, J.; Herranz, J.; Dodelet, J. P. *Nat. Commun.* **2011**, *2*, 416.
(42) Zhang, X.; Sun, X.; Chen, Y.; Zhang, D.; Ma, Y. *Mater. Lett.* **2012**, *68*, 336−339.
(43) Pylypenko, S.; Mukherjee, S.; Olson, T. S.; Atanassov, P. *Electrochim. Acta* **2008**, *53*, 7875−7883.
(44) Mo, Z.; Peng, H.; Liang, H.; Liao, S. *Electrochim. Acta* **2013**, *99*, 30−37.
(45) Zhang, S.; Liu, B.; Chen, S. *Phys. Chem. Chem. Phys.* **2013**, *15*, 18482.
(46) Wang, H.; Bo, X.; Luhana, C.; Guo, L. *Electrochem. Commun.* **2012**, *21*, 5−8.
(47) Guo, H. L.; Su, P.; Kang, X.; Ning, S. K. *J. Mater. Chem. A* **2013**, *1*, 2248.
(48) Ghosh, K.; Kumar, M.; Maruyama, T.; Ando, Y. *Carbon* **2010**, *48*, 191−200.
(49) Choudhury, D.; Das, B.; Sarma, D. D.; Rao, C. N. R. *Chem. Phys. Lett.* **2010**, *497*, 66−69.
(50) Lai, L.; Potts, J. R.; Zhan, D.; Wang, L.; Poh, C. K.; Tang, C.; Gong, H.; Shen, Z.; Lin, J.; Ruoff, R. S. *Energy Environ. Sci.* **2012**, *5*, 7936−7942.
(51) Kim, H.; Lee, K.; Woo, S. I.; Jung, Y. *Phys. Chem. Chem. Phys.* **2011**, *13*, 17505−17510.
(52) Qiao, J.; Xu, L.; Ding, L.; Zhang, L.; Baker, R.; Dai, X.; Zhang, J. *Appl. Catal., B* **2012**, *125*, 197−205.
(53) Guo, C. Z.; Chen, C. G.; Luo, Z. L. *J. Power Sources* **2014**, *245*, 841−845.